

Carbonaceous aerosol (Soot) measured in the lower stratosphere during POLARIS and its role in stratospheric photochemistry

A. W. Strawa,¹ K. Drdla,¹ G. V. Ferry,¹ S. Verma,² R. F. Pueschel,¹ M. Yasuda,³ R. J. Salawitch,⁴ R.S. Gao,⁵ S. D. Howard,⁶ P. T. Bui,¹ M. Loewenstein,¹ J. W. Elkins,⁷ K. K. Perkins,⁸ and R. Cohen⁹

Abstract. This paper describes recent measurements of carbonaceous aerosol made by wire impactors during the Photochemistry Ozone Loss in the Arctic Region in Summer (POLARIS) campaign and assesses their role in stratospheric photochemistry. Ninety-five percent of the carbonaceous aerosol collected during this campaign was in the form of black carbon aerosol (BCA), or soot. A new method of analyzing impactor samples is described that accounts for particle bounce and models the BCA as fractal aggregates to modify the aerodynamic collection efficiency and determine particle surface area. Results are compared to previously used methods. The new method results in an increase in the measured BCA number density of 4 times, surface area density of ~15 times, and an increase in mass loading of 6.15 times over one previously used approach. Average values of number, surface area, and mass densities are 0.06 no./cm³, 0.03 μm²/cm³, and 0.64 ng/m³, respectively. BCA number densities are ~1% of total aerosol number density, and BCA surface area density is ~10% of the measured sulfuric acid aerosol surface area. Including heterogeneous reactions on BCA in a photochemical model can affect photochemistry leading to renoxification and increased ozone depletion. However, these predicted effects are not supported by the POLARIS observations, in particular, the NO_x/NO_y ratios. The laboratory data is not conclusive enough to determine to what extent the heterogeneous reaction is catalytic or carbon consuming. Including catalytic reactions on BCA does not statistically improve the agreement between model and measurement in any of the several scenarios considered. Furthermore, if the reactions cause even partial carbon oxidation, the BCA would be consumed at a rate inconsistent with POLARIS observations. These inconsistencies lead us to conclude that the presence of BCA in the stratosphere did not affect stratospheric photochemistry during POLARIS.

1. Introduction

The presence of black carbon aerosol (BCA) in the stratosphere and upper troposphere has been observed and documented for many years and with different instruments [cf. *Pueschel et al.*, 1992; *Hansen and Rosen*, 1984]. However, due to the sparseness of measurements, the sources, sinks, and lifetime of BCA in the stratosphere is poorly

known. Recent modeling studies have shown that including heterogeneous reactions on BCA can improve agreement between model predictions and measurements in both the troposphere [*Hauglustaine et al.*, 1996] and stratosphere [*Lary et al.*, 1997]. *Lary et al.* [1997] included the reactions of HNO₃ and NO₂ on carbon particles in atmospheric model calculations. They used a reaction probability γ for HNO₃ conversion to NO_x (= NO + NO₂) of 2.8×10^{-2} and BCA surface areas from 0 to 10 μm²/cm². They found a major impact on nitrogen partitioning and on ozone chemistry in the stratosphere and troposphere. *Bekki* [1997] used enhanced values of BCA surface area in calculations of the midlatitude stratosphere to explain the observed ozone depletion in that region. Using a two-dimensional photochemical model, *Bekki* [1997] was able to reproduce much of the lower stratospheric ozone trends by employing heterogeneous reactions of ozone on BCA. The limitation of these studies is that they used estimates of BCA surface areas and assumed catalytic reactions. *Gao et al.* [1998] used O₃ abundances measured in a jet engine exhaust plume to estimate an upper limit of the value of the reaction probability surface area product, γSA , at 4.5×10^{-5} and 2.9×10^{-3} for the reduction of O₃ and NO₂, respectively. They also discussed the possibility that BCA would be coated by H₂SO₄ in the exhaust plume.

As part of the Photochemistry of Ozone Loss in the Arctic Region in Summer (POLARIS) campaign, measurements were made of BCA and many other quantities that allow a more specific study of the problem. The POLARIS campaign

¹National Aeronautics and Space Administration - Ames Research Center, Moffett Field, California

²Science Systems and Applications, Inc., Moffett Field, California.

³San Jose State University, San Jose, California.

⁴Jet Propulsion Laboratory, Pasadena, California.

⁵Aeronomy Laboratory, National Oceanic and Atmospheric Administration, Boulder, Colorado.

⁶Symtek, Moffett Field, California.

⁷Climate Monitoring and Diagnostics Laboratory, National Oceanic and Atmospheric Administration, Boulder, Colorado.

⁸Department of Earth and Planetary Science, Harvard University, Cambridge, Massachusetts.

⁹Department of Chemistry, University of California, Berkeley, California.

Copyright 1999 by the American Geophysical Union.

Paper number 1999JD900453.

0148-0227/99/1999JD900453\$09.00

focused on conditions of continuous solar exposure, especially the effect on nitrogen radicals (NO_x) which are central to ozone depletion. The goal of this paper is to assess the role of BCA in stratospheric ozone chemistry using data obtained during the POLARIS mission and computer simulations.

The critical role of sulfuric acid aerosol in stratospheric ozone depletion is well established [cf. *Fahey et al.*, 1993; *Gao et al.*, 1997]. Chemical reactions that take place on the sulfuric acid aerosol, in particular, the hydrolysis of N_2O_5 , transfer nitrogen out of the reactive nitrogen species, NO_x , and into the HNO_3 reservoir species. One of the most effective means of studying nitrogen partitioning is by examining the ratio of NO_x within the total reactive nitrogen reservoir, $\text{NO}_y (= \text{NO}_x + \text{NO}_3 + \text{HNO}_3 + \text{ClONO}_2 + 2\text{N}_2\text{O}_5 + \dots)$. Including heterogeneous reactions on sulfate aerosol in computer models has generally brought better agreement between measured and computed $\text{NO}_x / \text{NO}_y$ ratios. The impact of BCA on ozone depletion is felt through heterogeneous reactions that modify the partitioning between reactive and reservoir nitrogen species and that involve ozone directly. BCA may transfer nitrogen out of the reservoir HNO_3 species and into NO_x through the re-nitrication reaction:



This reaction acts in opposition to the heterogeneous sulfate reactions.

In the laboratory, *Thlibi and Petit* [1994] found that the reduction of HNO_3 to NO occurred on carbon. *Rogaski et al.* [1997] found that the major products of the heterogeneous reaction of HNO_3 with BCA were H_2O , NO_2 , and NO and reported an uptake coefficient of 3.8×10^2 . They measured two NO_x molecules produced for every three HNO_3 molecules adsorbed. More recently, however, *Choi and Leu* [1998] investigated the uptake and decomposition of HNO_3 on carbon black surfaces. Observations were made under stratospheric conditions of $P(\text{HNO}_3) \sim 10^2$ Torr and $T = 220$ K. Carbon black (Degussa FW2), graphite, hexane soot and kerosene soot samples were used as surrogate black carbon aerosol surfaces. They found that all black carbon samples tested at stratospheric conditions showed no reactivity towards nitric acid, but only limited physical absorption. NO_2 can be reduced on carbon aerosol to produce NO :



Further reaction of NO can lead to indirect ozone depletion. [*Lary et al.*, 1997] This reaction is independent of sunlight and can occur whenever carbon aerosol is present. *Tabor et al.* [1993,1994] report an uptake coefficient for NO_2 of 4.8×10^{-2} . *Thlibi and Petit* [1994] also found that NO_2 was reduced on solid amorphous carbon to yield NO . *Rogaski et al.* [1997] measured the uptake coefficient for NO_2 as 0.11 ± 0.04 . *Tabor et al.* [1994] reported 0.064 ± 0.02 and observed production of NO with initial conversion of 100%, but uptake of NO_2 and percent conversion to NO decreased with time.

Ozone losses may also occur through more direct interaction of ozone with BCA through the reaction



DeMore et al. [1997] and *Fendel and Ou* [1993] recommend a reaction probability for O_3 on soot of 3×10^2 . On the other hand, *Fendel et al.* [1995] found the reaction probability to be only about 10^{-4} . They concluded that carbon particles present in the stratosphere might be a significant sink for ozone. *Stephens et al.* [1986] measured an uptake coefficient of O_3 on carbon between 10^{-3} and 10^{-5} depending on carbon sample surface history, with CO , CO_2 , and O_2 as products. The presence of these products suggests that the ozone reaction on carbon is, at least in part, noncatalytic.

This paper discusses the measurement of BCA by the Ames Wire Impactors and assesses the role of BCA in stratospheric photochemistry. A new method of analyzing impactor samples is described that accounts for particle bounce and models the BCA as fractal aggregates to modify the aerodynamic collection efficiency and determine particle surface area. Results from the present analysis are compared with previous techniques and with BCA surface area values used in previous model simulations. The photochemical trajectory model used in the present simulations is described. An assessment of the importance of heterogeneous BCA reactions is made by comparing modeled and measured NO_x/NO_y ratios and effects on ozone loss. Finally, the implications of mass-balancing these reactions on the lifetime of BCA particles in the stratosphere will be discussed.

2. The Ames Wire Impactor

The Ames Wire Impactor (AWI) has been used extensively in the past on such missions as AAOE, AASE, AASE II, ASHOE/MAESA, and POLARIS to sample stratospheric aerosol. It has proven to be an accurate and reliable means for obtaining atmospheric aerosol size distributions, and sulfate and BCA burdens. The sampler consists of palladium and/or gold wires of 75- and 500- μm diameter that are strung across support rings. The wires are carbon coated and modules are assembled in a class 100 clean room. Up to six modules are mounted on the wingtip of the ER-2. Each module has the capability of holding several rings with several wires on each ring. The modules are exposed to the free stream by pre-selected triggers of time, altitude, or aircraft position. Aerosol particles suspended in the ambient air impact on the wires. A new automated sample actuation system was designed, fabricated, and successfully used to retrieve data during the POLARIS campaign. Samples were exposed typically for 3 min. Particles stick to the wire upon impact by virtue of van der Waals forces. After exposure, the wires are retracted into sealed modules containing concentrated ammonia vapor. The ammonia combines with the sulfuric acid aerosol to form ammonium sulfate which is very stable under laboratory conditions and allows for the sample to be stored indefinitely.

Particles are manually identified, counted, and sized using a Hitachi S-4000 field emission scanning electron microscope. Under the conditions used for imaging, the lateral resolution of the microscope is better than 10 nm. Particles are viewed at magnifications suitable to the size of the particle, between 1000 and 50,000 times. Where appropriate, a determination of the particle elemental composition is made using X-ray dispersive analysis. Uncertainty is proportional to the particle concentration because the error due to sampling statistics is much greater than the best estimate of uncertainties due to other factors such as particle sizing, collection efficiency, ambient speed,

and temperature. Typical uncertainties for the BCA samples collected during POLARIS are ~70%. These seemingly high uncertainties are due to the sparseness of BCA particles in the stratosphere (~0.06 per cm³ or 1% of total aerosol) which are subsequently collected by the AWI.

Their morphology and appearance of higher contrast in the electron beam identify carbonaceous particles. A composite of electron micrographs of carbonaceous particles collected during the POLARIS campaign is shown in Figure 1. The magnification of each particle is 50,000 times. For reference, each frame has the approximate physical dimensions of 700

nm by 700 nm. The vast majority of carbonaceous particles can be identified by their fractal geometry. There is a small percentage, < 5%, that have the contrast indicative of carbon but which have a more amorphous shape than the typical fractal particles. One such particle is represented in Figure 1*l*. X-ray energy dispersive analysis confirms that these particles do not contain minerals. These particles may be organic carbon particles or they may be fractal particles that have been covered by some substance. They are treated in our calculations as BCA particles.

Analysis of wire impactor samples accounts for changes in

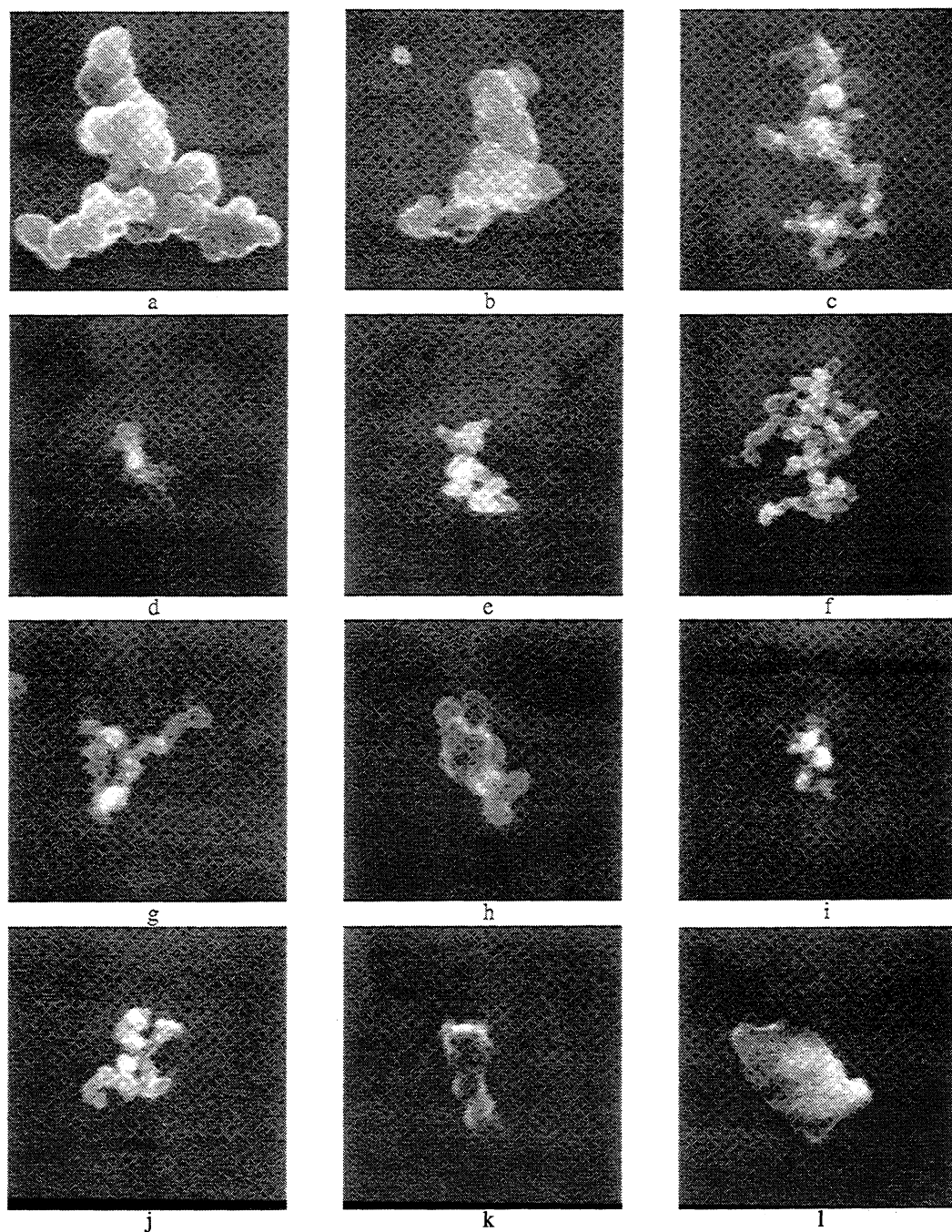


Figure 1 Composite of electron micrographs of carbonaceous particles collected during POLARIS. Images (a) through (k) are of fractal aggregates. Image (l) is an amorphous carbon particle. Fractal aggregates made up over 95% of the carbonaceous particles collected during POLARIS. For reference, each image represents approximately 700 nm by 700 nm in physical dimension.

size due to relative humidity [Steele and Hamill, 1981], for conversion of sulfuric acid droplets to ammonium sulfate, and for the collection efficiency of the wire. Much theoretical and experimental work has been done in the past to derive reasonably accurate collection efficiencies for impactor wires and plates under conventional collection conditions. Lem and Farlow [1977] have extended the relations developed by Wong *et al.* [1955] to typical ER-2 and DC-8 collection conditions for the collection of liquid sulfuric acid solution droplets, typical of the particles collected in the stratosphere and upper troposphere. The Lem and Farlow [1977] corrections have subsequently been applied to the theories of Suneja and Lee [1974] and Dunn and Renken [1987]. This is referred to as the liquid sphere method. In this report, we are interested in collecting and analyzing BCA whose aerodynamic forces differ from those of a sphere and whose material properties result in a tendency for particles to bounce off the wires.

Previously, two techniques have been used to determine BCA loading from AWI samples. Pueschel *et al.* [1992] used an average of the long and short dimension of the particle to estimate the aerodynamic diameter and used the liquid sphere method to determine the collection efficiency of the particles. Particle density was adjusted to account for the fact that the sphere designated by the average diameter was not completely filled by BCA monomers. The surface area was calculated as π times the average diameter squared. Blake and Kato [1995] used an average diameter determined as in the liquid sphere method and 100% aerodynamic collection efficiency was assumed, which should yield a lower limit on the number of particles collected. Neither method considered the effects of particle bounce. The analysis of Blake and Kato [1995] recognized that BCA was a fractal aggregate but attempted to get an improved estimate of the BCA surface area by assuming that the volume of a sphere, as determined by the liquid sphere method, was completely taken up by 20-nm monomers. The surface area calculated in this way gives an overestimate of the actual surface area. We have recently developed an analysis technique that corrects the aerodynamic collection efficiency and estimates the adhesion probability based on best available data and considers the fractal nature of the BCA in estimating surface area.

The liquid sphere theory relates the aerodynamic collection efficiency of liquid spheres to the Stokes parameter. The Stokes parameter can be defined as an explicit function of the aerodynamic diameter as

$$St = \frac{C_C \rho_p V_p v}{3\pi\mu_g D_{ae} D_w} \quad (1)$$

where ρ_p is the particle density, V_p is particle volume, D_{ae} is the aerodynamic diameter, D_w is collector wire diameter, v is the airstream velocity, μ_g is the gas viscosity,

$$C_C = 1 + \frac{2\lambda_g}{D_p} \left[1.23 + 0.41 \exp\left(-0.44 \frac{D_p}{\lambda_g}\right) \right] \quad (2)$$

is the Cunningham slip factor, and λ_g is the mean free path. We have adapted this theory by determining an appropriate value for the aerodynamic diameter and for this we use fractal theory.

BCA have different aerodynamic characteristics than liquid spheres and they are solid and are likely to bounce when impacting a solid surface. As can be seen in Figure 1, the BCA particles are characterized by an aggregate structure of smaller spherules, called monomers, that range from 50 nm to 70 nm in diameter. One can see that the sphere that encloses the particle is not completely filled with material so that the mass of a BCA aggregate is less than that of a sphere. This mass deficit as well as the different aerodynamic characteristics of the BCA particle must be taken in to account to obtain an accurate measure of BCA loading and surface area. In the present theory, BCA is modeled as a fractal aggregate.

Wire impactors offer the advantage that the actual particles are retained and can be individually analyzed for size, morphology, and elemental composition. On the basis of observations of many BCA particles collected over the past several years, we find that the morphology of stratospheric and upper tropospheric BCA is very similar to that observed for other types of BCA originating from combustion processes, from diesel exhaust soot to biomass burning, all of which can be described as fractal aggregates. The formation of aerosol aggregates has been described in terms of cluster-cluster models [Jullien, 1987]. Previous studies on BCA formation have determined that a diffusion limited cluster-cluster mechanism dominates. Referring to Figure 1, we can define two characteristic dimensions to the particle: the average diameter of a monomer, d_0 , and the geometric diameter, D_{ge} , defined as the diameter of the smallest sphere that encloses the entire aggregate. These dimensions can be used to estimate the number of monomers in a fractal, N , and the aerodynamic diameter, D_{ae} , by the relations [Magill, 1991; Mandelbrot, 1982]

$$N = \left(D_{ge}/d_0\right)^f \quad (3)$$

$$D_{ae} = d_0 \left(D_{ge}/d_0\right)^{(f-1)/2} \quad (4)$$

where f is defined as the fractal dimension. The relation in equation (4) is derived from scaling arguments. Laboratory calibrations are needed to confirm this relationship. The mass of a fractal aggregate is given by

$$M_{ae} = \frac{N}{6} \rho_0 \pi d_0^3 \quad (5)$$

where ρ_0 is the density of a monomer.

Typical mean values of fractal dimension for aggregates formed by diffusion limited cluster-cluster mechanisms are between 1.8 and 2.1. [Jullien *et al.*, 1987] After consideration of many experiments and simulations, Nyeki and Colbeck [1995] took the fractal dimension of BCA particles to be 1.91 in their study, and we follow their example in this work.

The second factor involved in the impactor collection efficiency is accounting for particle bounce by estimating the adhesion probability. Ellenbecker *et al.* [1980] investigated the adhesion probability of fly ash with impactor samples experimentally and theoretically and plotted adhesion probability α versus kinetic energy κ . A power law fit to their data was used in our formulation:

$$\alpha = 1.46 \times 10^{-4} \kappa^{(-0.246)} \quad (6)$$

We feel this is justified because their results are in a kinetic energy range of 10^{-16} to 10^{-10} m/s² and our particles' kinetic energy is typically in the range 10^{-15} to 10^{-12} m/s². Clearly, however, experiments must be conducted to determine the adhesion probability of particles typically found in the stratosphere.

Surface irregularity, as it pertains to surface area and reaction surface areas, is one of the most important characteristics of materials. Surface areas, as a function of material mass, are derived from nitrogen adsorption using the BET technique and can be found in the literature [cf. Pfeifer and Anvir, 1983; Zerda et al., 1992; Xu et al., 1996; Kirk-Othmer, 1992]. The relationship is

$$SA_{ag} = F_{SA} M_{ag}. \quad (7)$$

The surface area to mass ratio F_{SA} is typically a function of the monomer size, fractal dimension, surface conditions, adsorbate cross sections, and environmental conditions. For the purposes of determining the appropriate F_{SA} we chose data for carbon aggregate particles which most closely resembled those that were measured in POLARIS, other measurements made in the stratosphere [Pueschel et al., 1997], and from combustion of fossil fuels [Nyeki and Colbeck, 1995; Chughtai et al., 1999; Akhter et al., 1985]. These carbon aerosol have a fractal dimension f of ~ 1.9 and monomer diameters between 30 and 120 nm. Surface area analysis has been carried out using other adsorbates such as argon, ethane, and propane [Zerda et al., 1992]. For the molecules of interest in this study, use of the nitrogen numbers seemed most appropriate. A compilation of data from Zerda et al. [1992] and Kirk-Othmer [1992] is shown in Figure 2 as F_{SA} plotted against d_0 . The relationship between F_{SA} and d_0 can be approximated by the relationship

$$F_{SA} = \frac{SA_{ag}}{M_{ag}} \approx \frac{6}{\rho_0 d_0}. \quad (8)$$

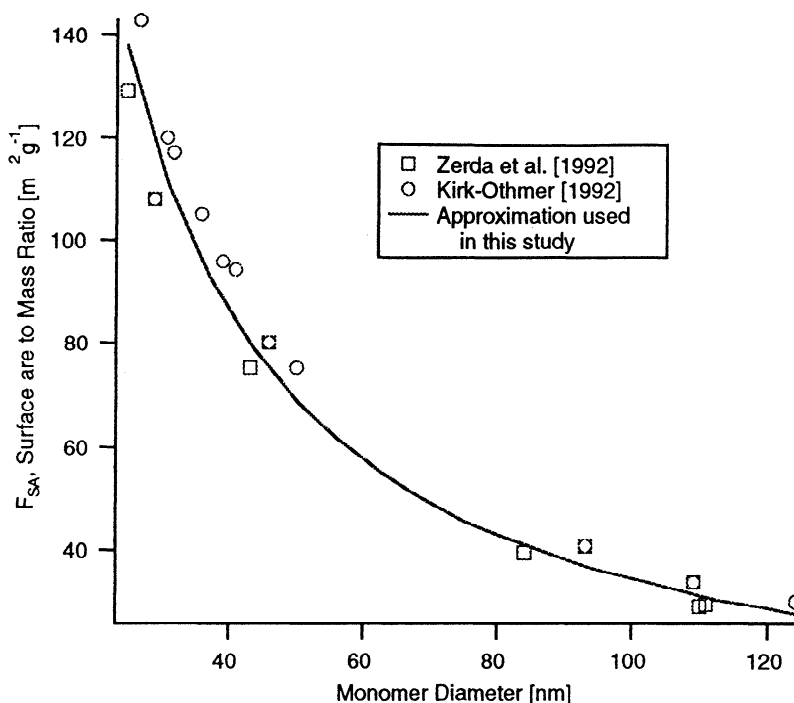


Figure 2 Surface area to mass ratio versus monomer diameter for fractal aggregates of fractal dimension about 2.

The surface area obtained with this relationship is approximately equal to the total surface area of all of the monomers, which is the theoretical limit, and suggests that very few monomers are shielded. In this case the aggregates are loosely packed as indicated by the fractal dimension of 2. The appearance of some aggregates in Figure 1 seems to indicate that some monomers are shielded but this may be an artifact of the resolution or focus of the SEM. Other aggregates in Figure 1 appear to be coated. X-ray analysis did not reveal any material in the aggregate other than carbon, however a coating several molecules thick is below the sensitivity limits of this technique. On the other hand, the surface area to mass ratios, F_{SA} , shown in Figure 2 are experimentally determined and give a much more accurate estimate of the surface area than that given in previous studies. The F_{SA} determined using this equation is ~ 60 m²/g for the monomer sizes observed in POLARIS (50-70 nm). This is lower than the value of 89 m²/g (n-hexane) and 65 m²/g (JP-8) used by Chughtai et al. [1999]. While the structure and monomer diameters of n-hexane soot ($d_0=80-100$ nm) [Akhter et al., 1984] was comparable with what was measured in this experiment, these values could not realistically be used because they were greater than the theoretical limit given by equation (8). Therefore we elected to use equation (8) in our formulation and consider it as an upper limit to the actual surface area of the aggregate.

Blake and Kato [1995] assumed that the entire volume of the sphere defined by the mean particle radius was taken up by 20-nm monomers and that the surface area of the aggregate was equal to the sum of all the monomer surface areas. This leads to an overestimation of the number of monomers and surface area of the aggregate and the present method is certainly more realistic.

The values of F_{SA} used to derive equation (8) are for carbon black that was treated by heating to 3000 K. Also, it is possible that there is some residue on the carbon surface of our aerosol that would change the probability of the reaction

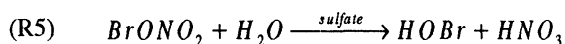
under consideration. For example, if the BCA were coated with sulfuric acid, the BCA might act like another sulfuric acid droplet. Certainly, more study is needed to better define the aerosol and the parameters used in this analysis and in computer simulations of the photochemistry.

3. The IMPACT Computer Model

The Integrated MicroPhysics and Aerosol Chemistry on Trajectories (IMPACT) model was used in this study to provide photochemical calculations along individual trajectories [Drdla, 1996]. Model photochemistry is based on Elliott *et al.* [1993], which uses a family approach with forward integration to provide stability with 1-hour model timesteps. For these studies, the model was configured with 57 species, grouped into 28 families, using 165 gas-phase reactions (of which 38 are photolysis reactions) with reaction rates based on DeMore *et al.* [1997]. Photolysis rates were calculated using a radiative transfer model that accounts for Rayleigh scattering [Salawitch *et al.*, 1994; Prather, 1981].

For each observation point, a backtrajectory has been determined from assimilated winds using the Goddard trajectory model [Schoeberl *et al.*, 1993]. The model is initialized at the start of the trajectory using ER-2 measurements of long-lived tracers (N_2O [Loewenstein *et al.*, 1990], O_3 [Proffitt *et al.*, 1993], NO_y [Gao *et al.*, 1999]); Cl_y and Br_y are initialized by combining ACATS measurements of organic source gases [Elkins *et al.*, 1996] with estimates of total chlorine [Montzka *et al.*, 1996] and total bromine [Wamsley *et al.*, 1998]. Ozone column and surface reflectivity are derived from TOMS (L. Moy and R McPeters, personal communication, 1998). The initial concentration of NO_x is set at 20% of NO_y ; the 10-day trajectories provide sufficient time for the model to repartition NO_y according to the chemistry.

The baseline model includes six sulfate aerosol heterogeneous reactions. During POLARIS, the only important sulfate reactions are



Constant reaction probabilities of 0.1 and 0.8, respectively [DeMore *et al.*, 1997], were assumed for these two reactions. Sulfate surface areas can be initialized based on one of two measurements, AWI or Focused Cavity Aerosol Spectrometer (FCAS) [Wilson *et al.*, 1992]. The AWI provides six 3-min average measurements per flight, while the FCAS instrument provides continuous measurements with high temporal resolution. FCAS measurements are therefore widely used for

ER-2 studies. FCAS sulfate surface area is used for most of the simulations in this paper to provide a basis for comparison with computations made in other studies. However, during POLARIS, the FCAS sulfate surface areas were on average 3.6 times higher than the AWI measurements. Simulations were also made using the AWI sulfate surface areas for the samples under consideration in this paper.

All three reactions on BCA, (R1)-(R3), have been incorporated into model. The reaction probabilities used in various runs are listed in Table 1. The maximum and minimum values were used to provide uncertainty estimates. For reaction (R1), the products are assumed to be 16% NO and 84% NO_2 , in accordance with previous modeling studies [Hauglustaine *et al.*, 1996; Bekki, 1997; Lary *et al.*, 1997]. However, preliminary studies showed no sensitivity to the product partitioning.

The ER-2 instrumentation simultaneously measures several nitrogen species: NO, with an accuracy F of $\pm 6\%$ [Del Negro *et al.*, 1999]; NO_y , $F = \pm 10\%$ [Gao *et al.*, 1999]; NO_2 using photolysis-chemiluminescence, $F = \pm 20\%$ [Del Negro *et al.*, 1999]; and NO_2 using laser-induced fluorescence, $F = \pm 20\%$. This allows direct determination of the $(NO+NO_2)/NO_y$ ratio, referred to here as the NO_x/NO_y ratio. As discussed elsewhere in this issue [Del Negro *et al.*, 1999], the two NO_2 measurements differ by on average 6%; for simplicity, the two measurement have been averaged for this study.

4. Results

During the POLARIS mission 150 samples were collected by the Ames Wire Impactor. Of these, 33 samples have been analyzed for sulfate aerosol distributions and 15 for BCA distributions. Table 2 is a summary of results of the BCA samples analyzed during POLARIS. The data are organized by sample number. BCA number, surface area, volume and mass densities as measured by the AWI are listed. Sulfate surface area density measured by both AWI and FCAS are also listed. Measurement means and uncertainties are listed for the AWI measurements. The large uncertainty in the BCA measurements is largely a result of the sparseness of the data. The samples provide a wide range of measurement conditions, in particular with respect to season and latitude as shown in Table 2. The altitude range is primarily limited to 18 - 21 km with one exception. Sample Z-26 collected on July 10, 1997, was taken at 15.5 km, well above the tropopause height. There appears to be a slight decrease in number density as altitude increases (~ 0.1 no./ cm^3 at 15.5 km and 0.07 no./ cm^3 at 20 km) that is not seen in the surface area, volume, and mass densities. All of the samples analyzed were north of $50^\circ N$ except for Z-75 sampled at $26.6^\circ N$. Within the uncertainty of the samples there appears to be no correlation

Table 1. Soot Reaction Parameters Used in IMPACT Model

Reaction	Reaction Probability (γ) Values			Reference(s)
	Standard	Minimum	Maximum	
(1) HNO_3	0.038	0.02	0.046	Rogaski <i>et al.</i> [1997]
(2) NO_2	0.11	4×10^{-4}	0.15	Rogaski <i>et al.</i> [1997]; Kalberer <i>et al.</i> [1996]
(3) O_3	10^{-3}	1.5×10^{-4}	3×10^{-3}	Rogaski <i>et al.</i> [1997]; Fendel <i>et al.</i> [1995]

Table 2. Measurement Conditions and Values for AWI Samples During POLARIS

Sample	Date	Latitude	Altitude, km	AWI BCA Values				AWI Sulfate:	FCAS Sulfate:
				Number Density, no./cm ³	Surface Area Density, $\mu\text{m}^2/\text{cm}^3$	Volume Density, $\mu\text{m}^3/\text{cm}^3$	Mass Density, ng/m ³	Surface Area Density, $\mu\text{m}^2/\text{cc}$	Surface Area Density, $\mu\text{m}^2/\text{cc}$
V-44	970430	64.1°N	18.9	1.82E-01	7.32E-02	8.91E-04	1.78E+00	1.20E-01	1.02E+00
V-45	970430	63.8°N	18.9	6.49E-02	9.54E-03	1.16E-04	2.32E-01	6.44E-02	1.01E+00
V-58	970502	69.9°N	19.2	3.36E-02	7.98E-03	9.71E-05	1.94E-01	1.91E-01	9.15E-01
V-60	970502	70.0°N	20.1	2.32E-02	6.23E-03	7.58E-05	1.52E-01	4.67E-01	7.92E-01
V-92	970629	57.3°N	17.9	6.04E-02	2.30E-02	2.93E-04	5.86E-01	2.40E-01	1.30E+00
Z-01	970630	66.9°N	18.1	9.43E-02	1.96E-02	2.38E-04	4.76E-01	6.32E-01	1.37E+00
Z-18	970707	89.4°N	18.9	3.68E-02	1.01E-02	1.23E-04	2.46E-01	3.69E-01	8.74E-01
Z-26	970710	65.2°N	15.5	9.86E-02	1.82E-02	2.21E-04	4.42E-01	2.74E-01	1.94E+00
Z-51	970914	64.6°N	19.3	3.61E-02	9.74E-02	1.02E-03	2.04E+00	2.81E-01	1.00E+00
Z-65	970918	88.4°N	19.8	3.99E-02	7.87E-02	5.99E-04	1.20E+00	2.93E-01	7.89E-01
Z-48	970919	64.5°N	19.2	2.68E-02	5.94E-03	7.23E-05	1.45E-01	2.58E-01	9.50E-01
Z-56	970919	64.5°N	19.2	5.32E-02	2.60E-02	2.46E-04	4.92E-01	2.39E-01	9.47E-01
Z-71	970921	49.6°N	19.5	2.62E-02	7.89E-03	6.31E-05	1.26E-01	4.04E-01	1.01E+00
Z-75	970921	26.6°N	20.6	1.11E-01	6.60E-02	4.28E-04	8.56E-01	3.52E-01	8.69E-01
Means				6.34E-02	3.21E-02	3.20E-04	6.40E-01	2.99E-01	1.06E+00
Uncertainty				46.8%	77.9%	78.1%	78.1%	15.2%	

Read 1.82E01 as 1.82x10⁻¹.

between the BCA measurements and latitude. The surface area density of sulfate measured by the AWI is $0.3 \mu\text{m}^2/\text{cm}^3$ in agreement with other measurements in volcanically quiescent periods by Poeschel *et al.* [1989] of $0.43 \mu\text{m}^2/\text{cm}^3$. Note that the FCAS sulfate surface area is systematically higher than that measured by AWI.

Figure 3 is a BCA surface area distribution from sample Z-71 collected on September 21, 1997, which is typical of our distributions. The sulfate surface area distribution is also shown to give some perspective of the relative magnitudes of sulfate aerosol and BCA present in the stratosphere.

Table 3 shows a comparison of methods for calculating the BCA parameters, the traditional liquid sphere approach and the present fractal method are applied to this data set. They are compared to values taken from Blake and Kato [1995]. Since the Blake and Kato values were normalized for STP we have adjusted them for comparison to our average altitude of 18.7 km by dividing by a factor of 11.6. The BCA number and mass density calculated by the present method are larger than the liquid sphere value on average by about a factor of 4 and 6.15, respectively. This is due primarily to including particle bounce effects in the collection efficiency. The fractal method increases the surface area density by ~15 which reflects taking into account the fractal nature of the aggregate.

As noted previously the surface area to mass ratio, F_{SA} , is an important parameter for fractal aggregates. F_{SA} for a liquid sphere is ~10 assuming a particle diameter of 300 nm. This agrees with the value of 11.4 listed for the liquid sphere method. The average value obtained with the present fractal method is 50. From Figure 2 this F_{SA} can be seen to correspond to a monomer size of ~68 nm. Using the total surface area and mass density from Table 2 of Blake and Kato [1995] a value for F_{SA} of ~139 is obtained which corresponds to a monomer diameter of 22 nm. Monomer diameters were measured from SEM photographs of particles collected during POLARIS. The monomer diameters were between 50 and 75 nm. Monomer diameters were also measured from samples collected during the AASE II, SPADE II, and GLOBE II

campaigns and found to be in the range of 45 to 75 nm. The monomer size measured during POLARIS was somewhat larger than the 30 to 50 nm diameter monomers found in aircraft exhaust [Poeschel *et al.*, 1997]. This suggests that an appropriate monomer diameter is between 50 and 75 nm for stratospheric BCA and supports the surface area values obtained in this work.

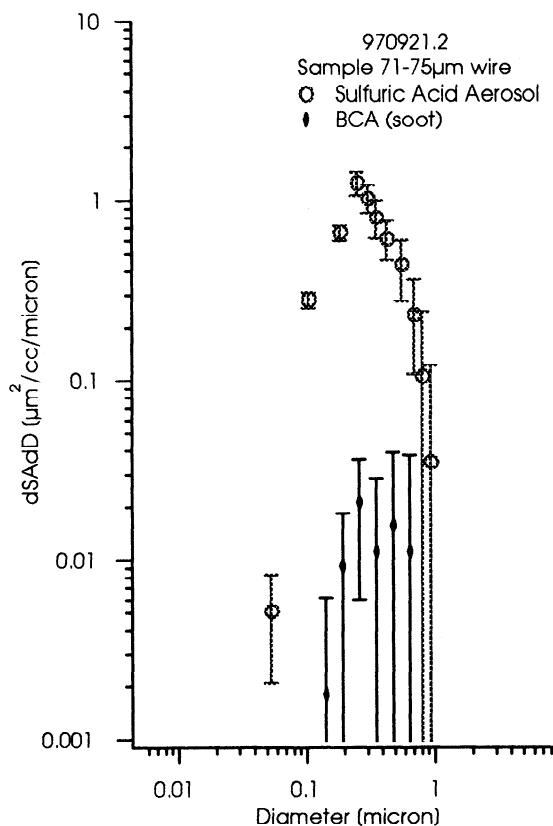


Figure 3 Typical BCA and sulfate surface area distributions collected during POLARIS on Sept. 21, 1997. Sample Z-71.

Table 3. Average Values at Stratospheric Conditions

Analysis Method	Soot Number Density, no./cm ³	SA, $\mu\text{m}^2/\text{cm}^3$	Mass, ng/m ³	SA/M, m ² /g	Sulfate SA, $\mu\text{m}^2/\text{cm}^3$
Liq. Sphere	0.0158	0.0016	0.14	11.4	0.29
B&K [1995] ¹	0.0058	0.0215	0.155	139	0.0215
Present Method	0.0634	0.0321	0.64	50	0.29
Model					
Bekki ²	unknown	0.02	0.05	450	unknown
Lary ³	unknown	0.2	unknown	unknown	unknown

¹ Blake and Kato [1995] values taken from Table 2 and adjusted from STP to 19 km for comparison with POLARIS data.

² Bekki [1997] values estimated from Figure 1. at 19 km. altitude

³ Lary *et al.* [1997] surface area taken from best agreement of ATMOS experiment and AutoChem model.

The POLARIS campaign occurred during a relatively quiescent volcanic period. The sulfate surface areas quoted here agree well with other volcanically quiescent values, but they are still much higher than the values quoted in the work of Blake and Kato [1995]. Table 3 shows that the BCA surface area is only 9.5% of the sulfuric acid surface area as opposed to the statement of Blake and Kato [1995] that the total surface area of BCA is the same order of magnitude as that of sulfuric acid aerosol during volcanically quiescent periods.

Bekki [1997] used a two-dimensional (2-D) model to calculate the distribution of BCA, and while his calculated values are in agreement with observations in the 12 to 14 km region, they are much lower in the 18 km region. The average altitude for the present set of data is 18.7 km and a typical Northern Hemisphere BCA loading used by Bekki is 0.02 ng/m^3 which is much lower than our measured value of 0.634 ng/m^3 . Hauglustaine *et al.* [1996] used a value for F_{SA} of $140 \text{ m}^2/\text{g}$ that may have influenced their results.

When comparing data obtained during the Atmospheric Trace Molecule Spectroscopy (ATMOS) Experiment with results from the AutoChem column model at 44.6° N latitude, Lary *et al.* [1997] obtained good agreement between model and observations with a BCA surface area density of $0.2 \mu\text{m}^2/\text{cm}^3$. Our average surface area is much lower at $0.031 \mu\text{m}^2/\text{cm}^3$ overall and our midlatitude ($45\text{--}64^\circ \text{ N}$) average was $0.033 \mu\text{m}^2/\text{cm}^3$. This overestimate of the BCA surface area would influence their study, increasing the apparent impact of BCA-catalyzed reactions on NO_x/NO_y ratios in the troposphere and stratosphere, and perhaps, accounts for the differences between their conclusions and the conclusions of this study.

4.1 NO_x/NO_y Ratio and the HNO_3 Reaction

Comparisons were made between modeled and measured NO_x/NO_y ratios, with and without BCA reactions, using the IMPACT model with the reactions and reaction probabilities listed in Table 1. Measured BCA surface areas from Table 2 were used to initialize the model. Initial sensitivity tests confirmed that model results are dependent only upon the BCA surface area, not the assumed BCA size distribution. For one data point, sample Z-18 collected on July 7, 1997, the NO_2 measurements were unavailable and therefore it was excluded from the NO_x/NO_y analysis. Both the 75- and 500-

μm wires were analyzed for sample Z48 collected on 19 Sept. 1997. Only the 75- μm wire numbers are included in this study.

Figure 4 shows that the baseline model (with sulfate and without BCA reactions) consistently underpredicts the NO_x/NO_y ratio, over a wide range of conditions. Only for one sample, Z-71, does the model exceed the measured value; the model is also close for Z-65. On average, the model value is 35% too low. In order to assess the ability of each model

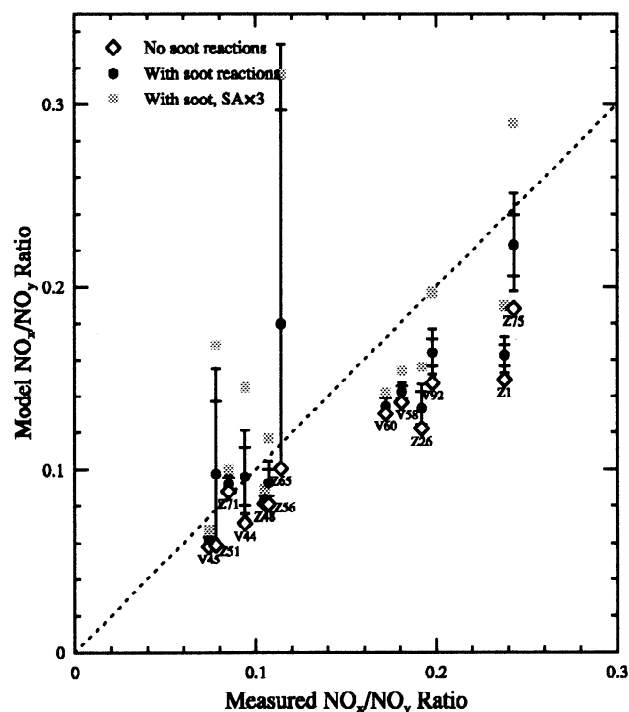


Figure 4 Comparison between measured and modeled values of $(\text{NO} + \text{NO}_2)/\text{NO}_y$ for each of the AWI BCA samples. Diamonds: baseline simulations (no BCA reactions). Circles: simulations including reactions (R1)–(R3) with measured BCA surface area. Squares: simulations including reactions (R1)–(R3) and BCA surface areas enhanced by a factor of three. The inner set of error bars reflects the statistical uncertainty associated with the measurement of BCA surface area; the outer set also includes the uncertainty in the reaction probabilities, see Table 1.

scenario to match the measured NO_x/NO_y ratio we calculated the rms deviation d for each scenario defined as

$$d = \sqrt{\frac{\sum (r_{\text{model}}/r_{\text{meas}} - 1)^2}{ns}} \quad (9)$$

where r is the NO_x/NO_y ratio for model and measurement respectively, and ns is the number of samples considered. This figure of merit tends to assume that the measurement is perfect, which is acceptable in this analysis and gives equal weight for all values of NO_x/NO_y . A lower value of d means better performance. For this scenario the value of d is 0.25. A summary of the rms deviations obtained from various model scenarios is shown in Table 4.

Adding the BCA reactions (R1)-(R3) increases the NO_x/NO_y ratio as expected; in particular, for samples with high BCA loadings (V-44, Z-51, Z-65, and Z-75) observable changes are predicted. The uncertainty bars are due to uncertainties in BCA surface area and in the assumed reaction probabilities. All three reactions are included in the simulations, but only (R1) influences the NO_x/NO_y ratio. Model increases in the NO_x/NO_y ratio do not, however, improve agreement with the measurements ($d = 0.25$). In particular, for samples with low initial NO_x/NO_y ratios, the scatter is greatly increased due to the high BCA surface area for two of the samples. Even taking into account the uncertainty in both BCA and the reaction probabilities, the majority of the data points do not match the measurements (8/13 underpredict, 1/13 overpredict).

An alternative method of evaluating reaction (R1) is to determine the BCA loading necessary to match the NO_x/NO_y for each point (Figure 5). These best fit values are of the same magnitude as the measured surface areas and have a similar degree of variability. However, the average value ($0.063 \mu\text{m}^2 \text{cm}^{-3}$) is twice as large as the measured average ($0.032 \mu\text{m}^2 \text{cm}^{-3}$) and the variability does not correlate with the measurements.

Increases in stratospheric BCA loading due to increases in air traffic would result in even more dramatic effects on stratospheric chemistry. Simulations were done with a three-fold increase in BCA surface area (Figure 4), consistent with the anticipated 5% annual increase in air traffic over the next 20 years [Schumann *et al.*, 1993]. Measurable increases in the NO_x/NO_y ratio are predicted for the majority of the samples, with a doubling for several points.

However, these changes in the NO_x/NO_y ratio translate into generally small effects on the ozone loss rate. On average,

Table 4. Summary of Correlation Coefficients for Various Simulations

Scenario	RMS Deviation, d	
	No BCA Reactions	All BCA Reactions
JPL97 ¹ , AWI sulfate	0.18	0.40
JPL97 ¹ , FCAS sulfate	0.25	0.25
JPL97 mod ² , FCAS sulfate	0.12	0.07

¹DeMore *et al.* [1997]

²JPL 97 chemistry with new reaction rates for OH+NO₂ and OH+HNO₃ reactions [Brown *et al.*, 1999a, b]

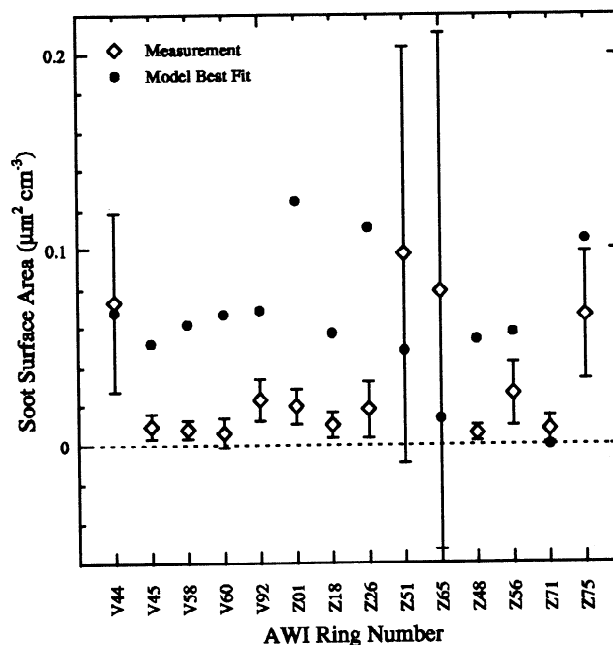


Figure 5 BCA surface areas necessary for model to match measured values of $(\text{NO} + \text{NO}_2)/\text{NO}_y$ with reactions (R1)-(R3) included, compared to measured BCA surface areas.

ozone is produced at a rate of 0.08 ppb/d when only reaction (R1) is included in the model. The most extreme effect, for the largest BCA loading, was an ozone production of 0.32 ppb/day. This is at least an order of magnitude smaller than the ozone loss rate in the absence of BCA reactions. These small values are due to the offsetting influences of the NO_x catalytic cycles, which become more effective with higher NO_x/NO_y ratios, and the other catalytic cycles (HO_x , ClO_x , BrO_x) which become less effective when high NO_x levels convert these other radicals to reservoir species [Wennberg *et al.*, 1994].

A decrease in sulfate surface area causes reaction (R4), N_2O_5 hydrolysis, to be less efficient, thus increasing the NO_x/NO_y ratio. Figure 6 shows model results using AWI surface areas, both with and without BCA reactions. Without the BCA reactions, the simulations are closer to the measurements overall than for the analogous simulations using FCAS sulfate surface area ($d=0.18$) than for the analogous simulations using FCAS sulfate surface area ($d=0.25$). Using both AWI sulfate and including the BCA reactions, however, generally causes the NO_x/NO_y ratio to exceed the measurements, causing d to increase to 0.40. This demonstrates that the NO_x/NO_y ratio is more sensitive to the magnitude of the sulfate surface area than it is to including the BCA reactions.

Recent laboratory studies have shown that the rates of relevant gas-phase reactions may differ from the recommendations of DeMore *et al.* [1997] in the stratosphere. The rate of the OH+NO₂ reaction is ~20% slower [Brown *et al.*, 1999a; Dransfield, *et al.*, 1999], and the OH+HNO₃ reaction is ~30% faster [Brown *et al.*, 1999b]. The effects of these reactions during the POLARIS campaign are discussed in more detail by Gao *et al.* [1999] and Osterman *et al.* [1999]. A set of simulations was done in which both of these new rates were incorporated (Figure 7). As expected, this

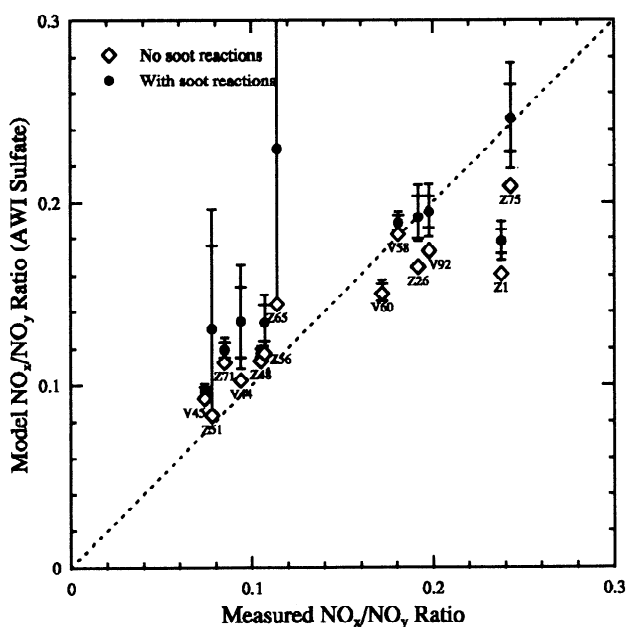


Figure 6 Same as Figure 4, except that the sulfate aerosol concentrations are initialized using AWI measurements, rather than FCAS measurements.

leads to higher NO_x/NO_y ratios and therefore better agreement with the measurements ($d=0.12$). When the soot reactions are also included, the uncertainty range for each point falls within 5% of the measurements, however, the overall fit is worse ($d=0.29$).

4.2 NO/NO_2 Ratio and the NO_2 Reaction

The model's predicted NO/NO_2 ratio matches the measurements within 10% at all points; on average the model is only 3% lower than the measurements. Both values are well within the combined measurement uncertainties. Adding reaction (R2) has no effect on the NO/NO_2 ratio ($<0.1\%$), even for a maximum reaction probability ($\gamma=0.11$) and maximum BCA surface area, because the gas-phase reactions are 4 orders of magnitude more rapid.

This small effect translates into negligible ozone depletion. Even at night, where NO_2 loss is equivalent to ozone loss [Lary *et al.*, 1997], sensitivity tests show that the impact is insignificant. Annual ozone loss rates due to this reaction are estimated to be at most 0.02% per year.

4.3 Ozone Reaction

Direct ozone loss, via reaction (R3), is found to have the most significant effect on ozone loss rates for the various BCA reactions during the POLARIS campaign. Figure 8 compares the net ozone production for the baseline simulation (gas-phase and sulfate reactions) over the 10-day trajectory with simulations that include the ozone reaction involving BCA. Significant ozone loss is predicted for air masses with high BCA loadings. In most cases, however, the impact of the BCA reactions (represented by the solid circles) tends to be small compared to the gas-phase reactions (represented by the diamonds), i.e., the solid circles are nearly equal to the diamonds.

Unlike most ozone destroying reactions, no sunlight is necessary for reaction (R3). In fact, the ozone loss rate on

BCA should only be dependent on the BCA surface area, allowing these calculations to be directly extrapolated to annual ozone loss rates. For air parcels with large BCA loadings, 0.2% per year losses are predicted; the average ozone loss enhancement is 0.07% per year. While this magnitude of ozone loss is consistent with Bekki [1997], the affected altitude is different. Bekki [1997] found ozone loss due to BCA limited to altitudes below 20 km, because the modeled BCA loading that they used peaked at 12–13 km. The POLARIS measurements of BCA loading imply that chemical signatures of BCA can extend to higher altitudes.

4.4 BCA Lifetimes

For each of the three BCA reactions, the reaction products have not yet been fully characterized; both the product stoichiometry and reaction mechanisms need to be better understood. In particular, extra oxygen needs to be accounted for in the reaction products. This has not been explicitly taken into account in any of the modeling studies. As will be discussed in this section, the fate of the extra oxygen determines whether the reactions can be effective over extended periods of time.

Consideration of reaction (R3), the ozone reaction, shows that as written (and as incorporated into the model in the previous simulations), it is not mass-balanced. One extra oxygen atom needs to be included in the reaction products, with four possible outcomes:

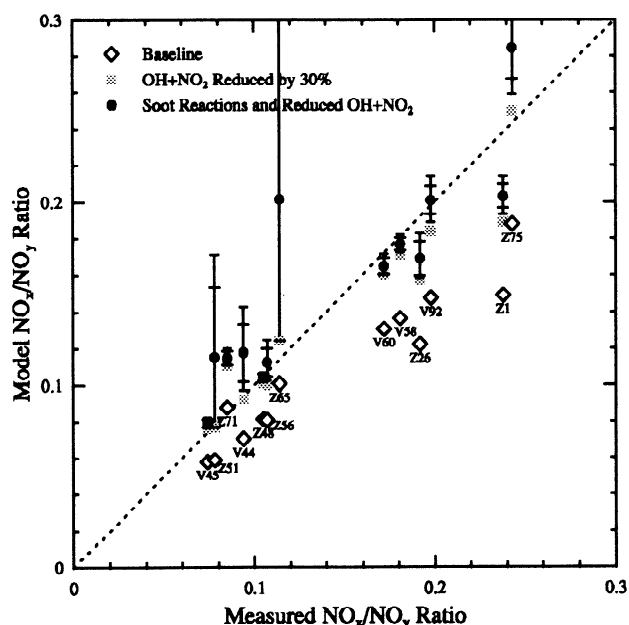
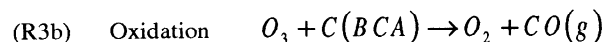
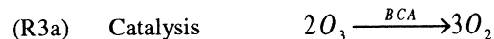


Figure 7 Same as Figure 4, except $\text{OH} + \text{NO}_2$ and $\text{OH} + \text{HNO}_2$ reaction rates are changed in accordance with Brown *et al.* [1999a,b]. Simulations initialized with FCAS sulfate surface area.

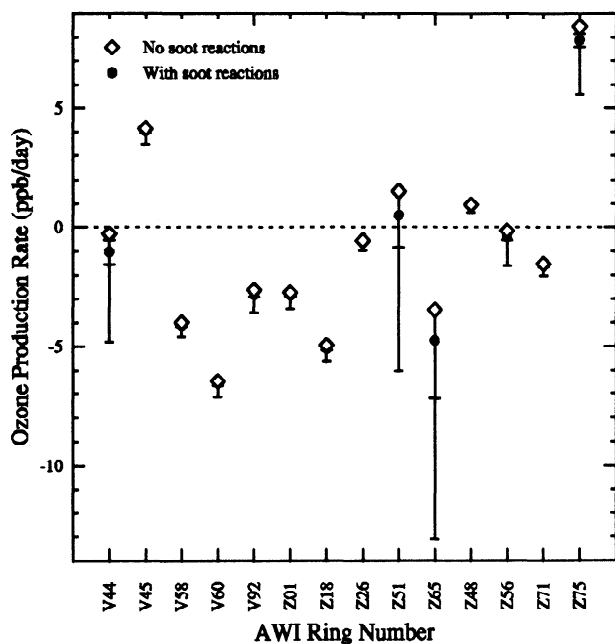


Figure 8 Net ozone production rate, due to both gas phase and heterogeneous reactions, over the ten-day trajectory. Diamonds: baseline simulations (no BCA reactions). Circles: simulations including reactions (R1)-(R3) with measured BCA surface areas. The inner set of error bars reflects the statistical uncertainty associated with the measurement of BCA surface area; the outer set also includes the uncertainty in the reaction probabilities, see Table 1.

It is likely that some combination of these four pathways may occur; the branching ratios could depend upon environmental conditions and the characteristics of the BCA surface.

Only (R3a), a purely catalytic reaction, can lead to sustained ozone depletion. With (R3b), the BCA particles will eventually be destroyed. On the other hand, (R3c) represents any reaction in which the surface is altered by irreversible uptake of oxygen; the oxygen is unlikely to be present on the surface as free oxygen atoms, but rather is likely to bond to surface carbon and form carbon-oxygen groups such as carboxylic acids [Smith *et al.*, 1988]. As the oxygen reacts with surface carbon, the surface will become poisoned (i.e., the reactivity is decreased). Reaction (R3d) is

considered a null reaction in the stratosphere, because an ozone molecule will immediately be regenerated in the presence of excess oxygen.

A literature review shows that various methods have been used to measure the relative contributions of these pathways, as outlined in Table 5. Simultaneous, accurate measurements of O_2 and O_3 allow direct determination of the ratio $\Delta O_3/\Delta O_2$ and thus the extent to which the reaction is catalytic. Gas-phase CO (or CO_2) measurements can be used to quantify pathway (R3b). The branching ratio of pathway (R3c) has been determined by measuring gas-phase CO and CO_2 generation as BCA samples are heated to the point where surface carbon-oxygen groups volatilize. Alternatively, the particulate mass can be monitored, although care must be taken to discriminate between mass increases due to oxygen uptake via (R3c) and mass loss due to (R3b). Pathway (R3c) can further be confirmed through FTIR spectral characterization of the surface groups, in particular, increases in carboxylic acids. Only pathway (R3d) cannot generally be detected because of rapid secondary reactions of the oxygen atom. As long as the secondary reactions lead to a null reaction, (R3d) will not even be measured as contributing to the reaction; however, if $[O_3] > [O_2]$ in the laboratory, extra O_2 will be generated, causing (R3a) to be confused with (R3d). Unfortunately, no one study has simultaneously quantified all four pathways, which is necessary to allow a rigorous check of the branching ratios. Furthermore, the studies do not agree with each other. However, all the available data show that this reaction is not purely catalytic. Estimates of carbon consumption via pathway (R3b) range from 0.5% to 40%.

Modeling studies, including the present study, have simplified this laboratory data, using a single reaction probability which is constant over time, implicitly via pathway (R3a). A first step toward considering the full reaction mechanism is to determine the effects of including pathway (R3b), which will lead to destruction of the BCA particles. The lifetime of carbon can be calculated from

$$\tau = \frac{\text{carbon mass}}{\text{carbon loss rate}} \quad (10)$$

$$\approx \frac{\text{soot mass}}{\text{soot surface area}} \frac{1}{f \gamma m_c \bar{\sigma}_{O_3} [O_3]}$$

where f is

Table 5. Laboratory Information on Branching Ratios of Reaction (R3)

Study	Duration of experiments, s	Measurement Technique	Result	Implied Branching Ratio
		$\Delta O_2/\Delta O_3$	1 (0.65-1.25)	(3a) = 0%
Stephens <i>et al.</i> [1986]	7200	$(\Delta CO + \Delta CO_2)/\Delta O_3$	0.2-0.4	(3b) = 20-40%
		γ variation with time	decrease from 10^{-3} to 10^{-5}	(3c) is poisoning surface
Smith <i>et al.</i> [1988]	180	$\Delta CO/\Delta O_3$	1/185	(3b) = 0.5%
		change in surface groups	increase in carboxylic acids	(3c) is occurring
Fendel <i>et al.</i> [1995]	20	change in soot mass	positive while exposed to O_3	(3c) is occurring
Smith and Chughtai [1996]	7800	change in soot mass $(\Delta CO + \Delta(\text{soot C}))/\Delta O_3$	net negative after exposure to O_3 0.64-0.97	(3b) also occurred (3a) = 3-36%

the branching ratio for pathway (R3b), g is the overall reaction probability for reaction (R3), A_N is Avogadro's number, m_C is the atomic mass of carbon (g), w_{O_3} is the mean velocity of an O_3 molecule (cm/s), and $[O_3]$ is the ozone concentration (cm^{-3}).

Using the AWI measurements of BCA and assuming $f=1.0$, the calculated lifetimes of BCA are 1 to 2 hours. Such a short lifetime is inconsistent with the observed stratospheric BCA loadings. AWI BCA volume is plotted against the mean age of air, determined from SF_6 measurements onboard the ER-2, in Figure 9 [Elkins *et al.*, 1996; Volk *et al.*, 1997]. Even for a smaller value of f , the carbon oxidation should produce an anticorrelation between BCA mass and the age of the air (assuming that no additional BCA is injected into the parcel), but none is observed in Figure 9. Ignoring the possibility that BCA is injected into the stratosphere, $f\gamma$ would need to be 10^4 times slower in order to maintain BCA volumes over the multiyear lifetimes. Even if f were assumed to be 0.005, γ would need to be 50 times slower, which is too slow to have a stratospheric impact.

This discussion assumes that the reaction pathways remain constant even over multiyear periods of time, as necessary to apply laboratory measurements to stratospheric models. However, any changes to the particle surface, in particular via pathway (R3c), would affect the reactivities. A similar calculation of the timescale for the particle surface to react yields a lifetime of the surface of only five minutes; the hundred-fold decrease in reactivity observed by Stephens *et al.* [1986] corresponds to an e-folding lifetime of 25 min. One consistent explanation of the data is that rapid poisoning reduces the overall reactivity, and in particular slows pathway (R3b), preventing the BCA particles from fully oxidizing.

A similar analysis is possible for reactions (R1) and (R2), which also both produce extra oxygen atoms that have not been accounted for. BCA lifetimes for these reactions, again assuming $f=1$, are between 11 and 55 hours. Therefore, even if these reactions occur on different sites than the ozone reaction, they are rapid enough to independently oxidize

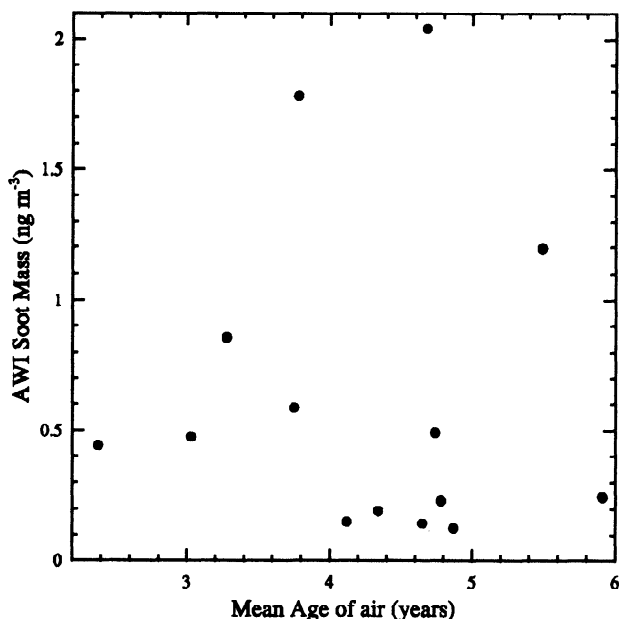


Figure 9 Cross plot of measured soot volumes and measured mean age of air. Mean age of air is determined from ACATS measurements of SF_6 .

atmospheric BCA particles. Given that all three reactions produce extra oxygen it is likely that these reactions actually compete for active sites. Rapid poisoning of the surface by ozone would then prevent the HNO_3 and NO_2 reactions from ever being effective.

Other atmospheric constituents are also likely to interact with soot particles, causing fundamental changes in surface characteristics and reactivity. In particular, both H_2O and H_2SO_4 are likely to poison the surface. Observations have shown that oxidized BCA particles become more hydrophilic [Chughtai *et al.*, 1996] may even have surface reactivities that more closely resemble stratospheric sulfate aerosol. For example, hydrophilic BCA particles tend to oxidize nitrogen, producing nitric acid [Mamane and Gottlieb, 1989; Tabor *et al.*, 1993 and references therein]. Furthermore, BCA may be rapidly coated with H_2SO_4 in aircraft plumes. Gao *et al.* [1998] proposed that H_2SO_4 coatings may have reduced the reactivities of measured soot particles. Karcher [1997] and Gleitsmann and Zellner [1998] have shown that such H_2SO_4 -coated BCA particles may trigger ice freezing and thus the formation of visible contrails.

In summary, studies of the long-term changes to BCA particles, including measurements of the reactivity and catalytic potential of highly oxidized particles are needed before the laboratory data can be incorporated into stratospheric models. Observations that oxidized BCA particles become more hydrophilic [Chughtai *et al.*, 1996], imply that the BCA surfaces may more closely resemble stratospheric sulfate aerosol. Also, better characterization of the differences between laboratory BCA particles and stratospheric BCA are needed.

5. Conclusions

Measurements of carbonaceous aerosol made by wire impactors during the POLARIS campaign are described and their role in stratospheric photochemistry is assessed. Impactor wires were analyzed for sulfuric acid aerosol and BCA distributions. More than 95% of the carbonaceous aerosol collected during this campaign was in the form of BCA or soot that displayed a fractal morphology ($D_{ge} \approx 300$ nm, $d_0 \approx 50$ -75 nm) suggesting origins in combustion processes. The BCA was analyzed using a new method that models the BCA as fractal aggregates and accounts for particle bounce. This resulted in an increase in the measured BCA number density of 4 times, surface area density of ~ 15 times, and an increase in mass loading of ~ 6 times over the previous approach. Average values of number, surface area, and mass densities are 0.0634 no./ cm^3 , 0.0321 $\mu m^2/cm^3$, and 0.64 ng/ m^3 , respectively. BCA number density is $\sim 1\%$ of total aerosol number density and BCA surface area density is about 10% of the measured sulfate surface area. This refutes the statement of Blake and Kato [1995] that the total surface area of BCA is of the same order of magnitude as that of sulfuric acid aerosol during volcanically quiescent periods. Previous modeling studies of heterogeneous reactions on BCA in the stratosphere have used values for BCA surface area that are much higher than those measured here; the high surface area produced significant effects of BCA on stratospheric photochemistry.

Including heterogeneous reactions on BCA as catalytic reactions in a photochemical model can lead to measurable changes in stratospheric chemistry. However, we found that the reactions affect stratospheric photochemistry in a way

inconsistent with other POLARIS observations. The primary problem is that measured BCA loading does not correlate with discrepancies between model and measurement in the baseline simulations. Including reaction (R1) leads to renoxification and to statistically poorer agreement between the modeled and measured ratios. We conclude that the heterogeneous reaction with HNO_3 (R1) is not significant during the POLARIS campaign and, in particular, is not responsible for the NO_x/NO_y discrepancies observed. Including reaction (R3) increased ozone depletion and annual ozone loss rates of up to 0.2% per year were predicted. The overall model/measurement agreement using the smaller AWI sulfate surface areas alone was better than in any simulation incorporating BCA heterogeneous reactions. This demonstrates that variations in the sulfate surface area were more successful in explaining NO_x/NO_y discrepancies than incorporating BCA reactions. The best model/measurement agreement was found in simulations with no BCA but where the gas-phase reaction rates were modified in accordance with recent studies [Brown et al., 1999a, b; Dransfield et al., 1999].

Consideration of the reaction pathways further suggests that heterogeneous reactions on BCA were not important during POLARIS. Laboratory data show that these reactions are not purely catalytic, and therefore either carbon is consumed by the reaction or the aerosol surface is altered. Calculations based on mass-balanced reactions resulted in BCA lifetimes of the order of hours, inconsistent with observations of BCA in the stratosphere.

By using an upper limit surface area, the paper demonstrates that heterogeneous reactions on BCA in the stratosphere are probably not important. This conclusion would also be true if we had used a smaller surface area in our calculations. Conversely, when the BCA surface area was allowed to vary so that the NO_x/NO_y ratio matched the measured ratio, the BCA surface area was much higher than the value we measured.

Further work is necessary to confirm these results. More study is necessary to insure that laboratory measurements of heterogeneous reactions are relevant to the stratosphere. One issue is the mechanism of the heterogeneous reactions; in particular whether the reactions are catalytic over extended periods. Similarly, it is necessary to confirm that the BCA being used in laboratory studies is similar to that found in the stratosphere. Changes in the surface behavior of BCA have implications beyond the reactions considered here. In particular, if the surface is hydrophilic or coated in sulfuric acid, the BCA may then oxidize nitrogen, resembling sulfate aerosols and may be important for cloud or contrail nucleation [Kärcher, 1997].

Finally, this study focused on arctic summer conditions, where gas-phase reactions are particularly efficient because of the extended solar illumination. In other regions of the stratosphere or during winter months, heterogeneous reactions are relatively more efficient, and BCA reactions may play a more important role. Furthermore, available measurements and global BCA climatologies suggest that BCA concentrations are elevated at lower altitudes. Thus studies similar to this need to be done under many different conditions.

Acknowledgments. The authors wish to thank R.D. May, C.R. Webster, M. Proffitt, M. Schoeberl, J. Margitan and J.C. Wilson for the use of their data and back trajectory calculations. In addition, the authors wish to thank the reviewers for many excellent

comments. K. Drdla is supported by the National Research Council. We gratefully acknowledge the support of NASA's Upper Atmosphere Research and Atmospheric Effects of Aviation Programs.

References

- Akhter, M.S., A.R. Chughtai, and D.M. Smith, The Structure of hexane Soot I: Spectroscopic studies, *Appl. Spectrosc.*, **39**, 1, pp. 143-153, 1985.
- Bekki, S., On the possible role of aircraft-generated soot in the middle latitude ozone depletion, *J. Geophys. Res.*, **102**, 10751-10758, 1997.
- Blake, D.F., and K. Kato, Latitudinal distribution of black carbon soot in the upper troposphere and lower stratosphere, *J. Geophys. Res.*, **100**, 7195-7202, 1995.
- Brown, S. S., R.K. Talukdar, and A. R. Ravishankara, Rate constants for the reaction $\text{OH}+\text{NO}_2+\text{M}\rightarrow\text{HNO}_3+\text{M}$ under atmospheric conditions, *Chem. Phys. Lett.*, **299**, 277-284, 1999a.
- Brown, S. S., R.K. Talukdar, and A.R. Ravishankara, Reconsideration of the rate constant for reaction of hydroxyl radicals with nitric acid, *J. Phys. Chem. A*, **103**, 3031-3037, 1999b.
- Choi, W. and M.-T. Leu, Nitric acid uptake and decomposition on black carbon (soot) surfaces: Its implications for the upper troposphere and lower stratosphere, *J. Phys. Chem. A*, **102**, 7618-7630, 1998.
- Chughtai, A.R., M.E. Brooks, and D.M. Smith, Hydration of black carbon, *J. Geophys. Res.*, **101**, 19505-19514, 1996.
- Chughtai, A.R., G.R. Williams, M.M.O. Atteya, N.J. Miller, and D.M. Smith, Carbonaceous particle hydration, *Atmos. Environ.*, **33**, 2679-2687, 1999.
- Del Negro, L. et al., Characterization of NO and NO₂ values during POLARIS using an improved in situ photolysis/chemiluminescence detector for NO₂, *J. Geophys. Res.*, this issue, 1999.
- DeMore, W.B., S.P. Sander, D.M. Golden, R.F. Hampson, M.J. Kurylo, C.J. Howard, and A.R. Ravishankara, C.E. Kolb, and M.J. Molina, Chemical kinetics and photochemical data for use in stratospheric modeling, in *Evaluation Number 12*, *JPL Publ.* 97-4, 1997.
- Dransfield, T.J., K.K. Perkins, N.M. Donahue, J.G. Anderson, M.M. Spengnether, and K.L. Demerjian, Temperature and pressure dependent kinetics of the gas-phase reaction of the hydroxyl radical with nitrogen dioxide, *Geophys. Res. Lett.*, **26**, 687-690, 1999.
- Drdla, K., Applications of a Model of Polar Stratospheric Clouds and Heterogeneous Chemistry, Ph.D. thesis, Univ. of Calif. at Los Angeles, 1996.
- Dunn, P.F., and K.J. Renken, Impaction of solid aerosol particles on fine wires, *Aerosol Sci. Tech.*, **7**, 97-107, 1987.
- Elkins, J.W., D.W. Fahey, J.M. Gilligan, G.S. Dutton, T.J. Baring, C.M. Volk, R.E. Dunn, R.C. Myers, S.A. Montzka, and P.R. Wamsley, Airborne gas chromatography for in situ measurements of long-lived species in the upper troposphere and lower stratosphere, *Geophys. Res. Lett.*, **23**, 347-350, 1996.
- Ellenbecker, M.J., D. Leith, and J.M. Price, Impaction and particle bounce at high Stokes numbers, *J. Air Pollut. Control Assoc.*, **30**(11), 1224-1227, 1980.
- Elliott, S., R.P. Turco, and M.Z. Jacobson, Tests on combined projection/forward differencing integration for stiff photochemical family systems at long time step, *Comput. Chem.*, **17**, 91-102, 1993.
- Fahey, D.W., et al., In situ measurements constraining the role of sulfate aerosols in mid-latitude ozone depletion, *Nature*, **363**, 509-514, 1993.
- Fendel, W.A. and A.S. Ott, *J. Aerosol Sci.*, **24**, S317-S318, 1993.
- Fendel, W., D. Matter, H. Burtscher, and A. Schmidt-Ott, Interaction between carbon or iron aerosol particles and ozone, *Atmos. Environ.*, **29**, 967-973, 1995.
- Gao, R.S., et al., Partitioning of the reactive nitrogen reservoir in the lower stratosphere of the southern hemisphere: Observations and modeling, *J. Geophys. Res.*, **102**, D3, 3935-3949, 1997.
- Gao, R.S., B. Kärcher, E.R. Keim, and D.W. Fahey, Constraining the heterogeneous loss of O₃ on soot particles with observations in jet engine exhaust plumes, *Geophys. Res. Lett.*, **25**, 3323-3326, 1998.

- Gao, R.S. et al., A comparison of observations and model simulations of NO_x/NO_y in the lower stratosphere, *Geophys. Res. Lett.*, **26**, 1153-1156, 1999.
- Gleitsmann, G., and R. Zellner, A modeling study of the formation of cloud condensation nuclei in the jet regime of aircraft plumes, *J. Geophys. Res.*, **103**, 19543-19555, 1998.
- Hansen, A.D.A., and H. Rosen, Vertical distribution of particulate carbon in the Arctic haze, *Geophys. Res. Lett.*, **11**, 381-384, 1984.
- Hauglustaine, D.A., B.A. Ridley, S. Solomon, P.G. Hess, and S. Madronich, HNO₃/NO_x ratio in the remote troposphere during MLOPEX 2, Evidence for nitric acid reduction on carbonaceous aerosols?, *Geophys. Res. Lett.*, **23**, 2609-2612, 1996.
- Jullien, R., *Comm. Condens. Matter Phys.*, **13**, 177-205, 1987.
- Jullien, R., R. Botet, and P.M. Mors, *Farad. Discuss. Chem. Soc.*, **83**, pp. 125-137, 1987.
- Karcher, B., and D.W. Fahey, The role of sulfur emissions in volatile particle formation in jet aircraft exhaust plumes, *Geophys. Res. Lett.*, **24**, pp. 389-392, 1997.
- Karcher, B., Heterogeneous chemistry in aircraft wakes: Constraints for uptake coefficients, *J. Geophys. Res.*, **102**, pp. 19,119-19,135, 1997.
- Kirk-Othmer, *Encyclopedia of Chemical Technology*, Fourth Edition, Vol. 4, J. Wiley, 1992.
- Lary, D.J., A.M. Lee, R. Toumi, M.J. Newchurch, M. Pirre, and J.B. Renard, Carbon aerosols and atmospheric photochemistry, *J. Geophys. Res.*, **102**, 3671-3682, 1997.
- Lem, H.Y., and N.H. Farlow, Efficiency of aerosol collection on wires exposed in the stratosphere, NASA TM 81147, 1977.
- Loewenstein, M., J.R. Podolske, and S.E. Strahan, Atlas Instrument Characterization: Accuracy of the AASE and AAOE Nitrous Oxide Data Sets, *Geophys. Res. Lett.*, **17**, 481-484, 1990.
- Magill, J., Fractal dimension and aerosol particle dynamics, *J. Aerosol Sci.*, **22**, Supp. 1, S165-S168, 1991.
- Mamane, Y. and J. Gottlieb, The Study of Heterogeneous Reactions of Carbonaceous Particles with Sulfur and Nitrogen Oxides using a Single Particle Approach, *J. Aerosol Sci.*, **20**, 575-584, 1989.
- Mandelbrot, B.B., *The Fractal Geometry of Nature*, W.H. Freedman and Co. 1982.
- Montzka, S.A., J.H. Butler, R.C. Myers, T.M. Thompson, T.H. Swanson, A.D. Clarke, L.T. Lock, and J.W. Elkins, Decline in the Tropospheric Abundance of Halogen from Halocarbons: Implications for Stratospheric Ozone Depletion, *Science*, **272**, 1318-1322, 1996.
- Nyeki, S., and I. Colbeck, Fractal dimension analysis of single, in-situ, restructured carbonaceous aggregates, *Aerosol Sci. Tech.*, **23**, 109-120, 1995.
- Osterman, G.B., et al., The partitioning of reactive nitrogen species in the summer arctic stratosphere, *Geophys. Res. Lett.*, **26**, pp. 1157-1160, 1999.
- Pfeifer, P., and D. Anvir, Chemistry in noninteger dimensions between two and three. I. Fractal theory of heterogeneous surfaces, *J. Chem. Phys.*, **79**(7), 3558-3565, 1983.
- Prather, M.J., Ozone in the upper stratosphere and mesosphere, *J. Geophys. Res.*, **86**, 5325-5338, 1981.
- Proffitt, M.H., K. Aikin, J.J. Margitan, M. Loewenstein, J.R. Podolske, A. Weaver, K.R. Chan, H. Fast, and J.W. Elkins, Ozone Loss Inside the Northern Polar Vortex During the 1991-1992 Winter, *Science*, **261**, 1150-1154, 1993.
- Pueschel, R.F., K.G. Snetsinger, J.K. Goodman, O.B. Toon, G.V. Ferry, V.R. Oberbeck, J.M. Livingston, S. Verma, W. Fong, W.L. Starr, and H.R. Chan, Condensed nitrate, sulfate, and chloride in Antarctic stratospheric aerosols, *J. Geophys. Res.*, **94**, D9, pp. 11,271-11,284, 1989.
- Pueschel, R.F., D.F. Blake, K.G. Snetsinger, A.D.A. Hansen, S. Verma, and K. Kato, Black Carbon (Soot) Aerosol in the Lower Stratosphere and Upper Troposphere, *Geophys. Res. Lett.*, **19**, 1659-1662, 1992.
- Pueschel, R.F., K.A. Boering, S. Verma, S.D. Howard, J. Goodman, G.V. Ferry, D.A. Allen, and P. Hamill, Soot aerosol in the lower stratosphere: Pole-to-pole variability and contributions by aircraft, *J. Geophys. Res.*, **102**, 13113-13118, 1997.
- Rogaski, C.A., D.M. Golden, and L.R. Williams, Reactive uptake and hydration experiments on amorphous carbon treated with NO₂, SO₂, O₃, HNO₃, and H₂SO₄, *Geophys. Res. Lett.*, **24**, 381-384, 1997.
- Salawitch, R., et al., The distribution of hydrogen, nitrogen, and chlorine radicals in the lower stratosphere: Implications for changes in O₃ due to emission of NO_x from supersonic aircraft, *Geophys. Res. Lett.*, **21**, 2547-2550, 1994.
- Schoeberl, M.R., S.D. Doiron, L.R. Lait, P.A. Newman, and A.J. Krueger, A Simulation of the Cerro Hudson SO₂ Cloud, *J. Geophys. Res.*, **98**, 2949-2955, 1993.
- Schumann, U., J. Strom, R. Busen, R. Baumann, K. Gierens, M. Krautstrunk, F.P. Schroder, and J. Stingl, In situ observations of particles in jet aircraft exhausts and contrails for different sulfur-containing fuels, *J. Geophys. Res.*, **101**, D3, 6853-6869, 1996.
- Smith, D.M., and A.R. Chughtai, Reaction kinetics of ozone at low concentrations with *n*-hexane soot, *J. Geophys. Res.*, **101**, 19607-19620, 1996.
- Smith, D.M., W.F. Welch, J.A. Jassim, A.R. Chughtai, and D.H. Stedman, Soot-Ozone Reaction Kinetics: Spectroscopic and Gravimetric Studies, *Appl. Spectrosc.*, **42**, 1473-1482, 1988.
- Steele, H.M., and P. Hamill, Effects of Temperature and humidity on the growth and optical properties of sulfuric acid-water droplets in the stratosphere, *J. Aerosol Sci.*, **12**, 6, 517-528, 1981.
- Stephens, S., M.J. Rossi, and D.M. Golden, The Heterogeneous Reaction of Ozone on Carbonaceous Surfaces, *Intl. J. Chem. Kin.*, **18**, 1133-1149, 1986.
- Suneja, S.K., and C.H. Lee, Aerosol filtration by fibrous filters at intermediate Reynolds numbers (≤ 100), *Atmos. Environment*, **8**, 1081-1094, 1974.
- Tabor, K., L. Gutzwiller, and M.J. Rossi, The heterogeneous interaction on NO₂ with amorphous-carbon, *Geophys. Res. Lett.*, **20**(14), 1431-1434, 1993.
- Tabor, K., L. Gutzwiller, and M.J. Rossi, Heterogeneous chemical kinetics of NO₂ on amorphous-carbon at ambient temperatures, *J. Phys. Chem.*, **98**(24), 6172-6186, 1994.
- Thlibi, J., and J.C. Petit, A study of the NO_x/Soot interaction in the temperature range 303-1223 K, paper presented at *Deutsche Forschungsanstalt für Luft- und Raumfahrt*, Köln, Germany, 1994.
- Volk, C.M., J.W. Elkins, D.W. Fahey, G.S. Dutton, J.M. Gilligan, M. Loewenstein, J.R. Podolske, K.R. Chan, and M.R. Gunson, Evaluation of source gas lifetimes from stratospheric observations, *J. Geophys. Res.*, **102**, D21, 25543-25564, 1997.
- Wamsley, P.R., J.W. Elkins, D.W. Fahey, G.S. Dutton, C.M. Volk, R.C. Myers, S.A. Montzka, J.H. Butler, A.D. Clarke, P.J. Fraser, Distribution of halon-1211 in the upper troposphere and lower stratosphere and the 1994 total bromine budget, *J. Geophys. Res.*, **103**, 1513-1526, 1998.
- Wennberg, P.O., R.C. Cohen, R.M. Stimpfle, J.P. Koplow, J.G. Anderson, R.J. Salawitch, D.W. Fahey, E.L. Woodbridge, E.R. Keim, R. Removal of Stratospheric O₃ by Radicals: In Situ Measurements of OH, HO₂, NO, NO₂, ClO, and BrO, *Science*, **266**, 398-404, 1994.
- Wilson, J.C., M.R. Stolzenburg, W.E. Clark, M. Loewenstein, G.V. Ferry, K.R. Chan, and K.K. Kelly, Stratospheric Sulfate Aerosol in and near the Northern Hemisphere Polar Vortex: The Morphology of the Sulfate Layer, Multimodal Size Distributions, and the Effect of Denitrification, *J. Geophys. Res.*, **97**, 7997-8013, 1992.
- Wong, J.B., W.E. Rantz, and H.F. Johnstone, Inertial impaction of aerosol particles on cylinders, *J. Applied Physics*, **26**(2), 244-249, 1955.
- Xu, W., T.W. Zerda, H. Yang, and M. Gerspacher, Surface fractal dimension of graphitized carbon black particles, *Carbon*, **34**, 2, 165-171, 1996.
- Yu, F. and R.P. Turco, The role of ions in the formation and evolution of particles in aircraft plumes, *Geophys. Res. Lett.*, **24**, pp. 1927-1930, 1997.
- Zerda, T.W., H.W. Yang, and M. Gerspacher, Fractal dimension of carbon-black particles, *Rubber Chemistry and Tech.*, **65**, 130-136, 1992.

A.W. Strawa, NASA Ames Research Center, Moffett Field, CA 94035. (astrawa@mail.arc.nasa.gov)

(Received December 4, 1998; revised June 10, 1999; accepted June 18, 1999.)